NTNU

Norwegian University of
Science and Technology

Comparing the Surface- and Interior Permanent Magnet Machine with Concentrated Windings for High Dynamic Applications

Lasse Kløvstad

Master of Energy and Environmental Engineering
Submission date: June 2017
Supervisor: Robert Nilssen, IEL

Norwegian University of Science and Technology
Department of Electric Power Engineering

Comparing the Surface- and Interior Permanent Magnet Machine with Concentrated Windings for High Dynamic Applications

Lasse Kløvstad
NTNU
Institute Of Electrical
Engineering
Trondheim, Norway
Email: lasse.klovstad@gmail.com

***Abstract*—This paper will compare the surface permanent magnet (SPM) machine to the interior permanent magnet (IPM) machine with fractional slot concentrated winding (FSCW). Key features is to achieve high field weakening with low losses, while keeping a high torque at rated speed. A walk through of essential theory concerning field weakening will be done. The application builder in COMSOL 5.2 was used to quickly do changes in the model. The Livelink Matlab extension was also used for post-processing the results and estimating the core losses.The results show that the I-shaped IPM machine has the lowest losses and both double layer and single layer winding can achieve high field weakening. The I-shaped rotor also has low total harmonic distortion and torque ripple. The V-shaped IPM rotor shows it difficult to optimize because of its many geometric variations and non linear behavior. The SPM machine has a higher power factor then the IPMs, due to the higher inductance in the IPM machines.**

***Keywords*—Optimal field weakening, eddy current loss, high dynamic applications, fractional slot concentrated winding, integer slot distributed winding, interior permanent magnet, surface permanent magnet.**

I. Introduction

High dynamic applications requires motors with high torque density, low inertia and ability for good field weakening performance. In addition the motor should have low torque ripple and high efficiency in all operating regions.

Many papers have investigated the high flux weakening performance of the FSCW SPM machine [1], [2] and [3]. The papers claim the abilities of 10:1 speed range on a constant power region. Not many of these motors have been tested over 5:1 speed range. The machines are design to have a field weakening index (FWI) equal to 1. Optimal Field weakening is achieved when the rated current is equal to the characteristic current I_{ch} [4]:

$$I_{ch} = \frac{\Psi_m}{L_d} \tag{1}$$

Field weakening index is defined as:

$$FWI = \frac{I_{ch}}{I_{rated}} \tag{2}$$

Traditionally IPM machines with integer slot distributed windings (ISDW) are used in high speed applications due to the extra saliency ratio the IPM gives. Saliency ratio is defined as:

$$\xi = \frac{L_q}{L_d} \tag{3}$$

IPM are more suited for high speed applications due to that the magnets are shielded by iron. The magnets can therefore handle more rotational forces then the SPM. The added saliency also provides reluctance torque and will increase the efficiency in the field weakening area. In [5] it is reviled that the CW IPM machines is inferior to the DW IPM in terms of generated torque and constant power region size.

On the other side not a lot of analyse has been done on the FSCW IPM machines and the full potential of this machine type is not fully reviled. It is a highly non-linear machine type and is more difficult to design and analyze [6]. In this paper a FSCW SPM machine designed for an offshore winch application will be compared to two types of FSCW IPMs. The goal is to achieve equal torque density at rated conditions and increase the field weakening range.

II. Theory

A. Basic Concepts

The produced torque in a machine is proportional to its size. [7]:

$$T = kD^2LAB_{AG} \tag{4}$$

Where D is the diameter and L is the axial length and k is a constant depending on the machine. Seen from this equation the torque is also proportional to the electric and magnetic loading. If the size is kept constant the torque can be increased either by magnetic or electric loading. This is usually done by the second method because the magnetic loading is independent of machine size and can usually maximum be 0.9 Tesla. Increasing electric loading is done by putting more current into the motor. The electric loading is given by:

$$A = \frac{6NI}{\pi D} \tag{5}$$

When changing the number of poles in a machine the ratio between the electrical and mechanicle angle changes. The electrical angle θ_e in a PMSM is defined as:

$$\theta_e = \frac{N_m}{2}\theta_m \tag{6}$$

Where N_m is the number of poles and θ_m is the mechanical angle. The angular frequency $\omega = 2\pi f$, where f is the frequency.

B. Total Harmonic Distortion

The total harmonic distortion (THD) is a measurement of a signals harmonic distortion. In this paper the THD is measured for the line voltage, where a low THD is wanted. The THD is calculated by this formula:

$$THD = \frac{\sqrt{V_2^2 + V_3^2 + V_4^2 ...}}{V_1} \tag{7}$$

Where V_1 is the main harmonic and $V_2, V_3 ...$ is the harmonic components in the signal. The harmonic components is obtain by a Fourier transform of the original signal. A pure sinusoidal signal will have a THD of 0 %.

C. Power Factor

The power factor (PF) is the ratio between real and reactive power flowing in the machine. It is preferred to have a high PF close to unity to maximize the real power. Having a low PF increases the converter cost since the cost of the converter is based on the apparent power. The PF is calculated based on the phase difference between the phase current and voltage. Since these signals can contain many harmonics, these signals are first Fourier transformed. Then the displacement power factor is calculated based on the phase difference of the main harmonics voltage and the current. While the total PF including the total harmonic distortion is calculated as:

$$PF = \frac{1}{\sqrt{1 + THD^2}} \cos \phi_1 \tag{8}$$

Where ϕ_1 is the angle between the main harmonic voltage and current. Seen from the formula the PF is reduced when the THD is increased. Therefore a low THD is optimal to increase the efficiency of the machine and converter.

D. Winding Types

There are mainly two types of windings; distributed and concentrated winding. Distributed windings (DW) is where coils of one phase is distributed over the magnet pole. Concentrated windings (CW) is traditionally where there is only one slot concentrated over a magnet pole. This basic concept is illustrated in figure 2. These windings can then be divided into double layer and single layer windings, illustrated in figure 1. Double layer winding is when two phases occupy one slot. Single layer is when only one phase occupy each slot.

Conventionally concentrated windings are non-overlapping and are used with fractional slots. Fractional slot concentrated windings are where the slot per pole per phase (q) is less then 1. Slot per pole per phase is defined as:

$$q = \frac{N_s}{N_{ph} \cdot N_m} \tag{9}$$

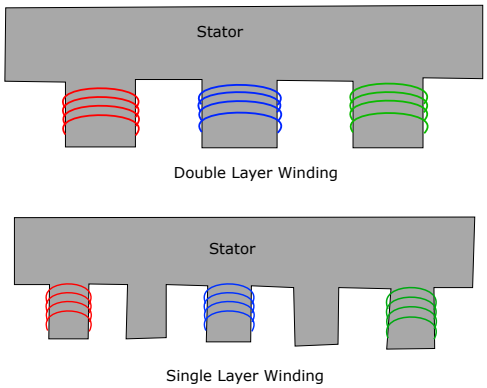

Fig. 1: Double layer and single layer windings

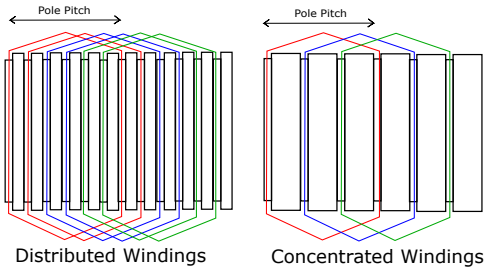

Fig. 2: Distributed and concentrated windings

Where N_s is number of slots and N_{ph} is number of phases. This paper only studies fractional slot concentrated windings where $q < 1$ and integer slot distributed windings (q is an integer).

E. Winding Layout Rules

There are many different combination when choosing how many slots and poles a machine can have. When choosing this some general rules must be followed [8]:

1) Number of poles need to be an even number.
2) Number of slots need to :
   a) be a multiple of the number of phases.
   b) If a double layer winding is used the number of poles can not be equal to the number of phases.
   c) If a single layer winding is used the number of poles can not be equal to the number of phases times two.

For FSCW the feasible region is $q \in [\frac{1}{4}, \frac{1}{2}]$ [8]. Outside these regions the winding factor is so low it would be a poor choice for slot and pole combination.

F. d- and q-axis Transformation

The Park transformation is commonly used in controlling synchronous motors. It assumes a sinusoidal flux density in the air gap. The main function of this transformation is to transform the 3 phase system, to a 2 phase system rotating with the synchronous frequency. First the a,b,c phase currents are transformed to the stationary reference frame, this is called the Clark Transform:

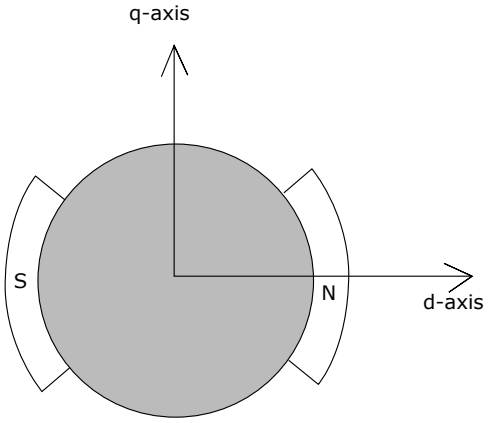

Fig. 3: Rotating dq system orientation

$$\begin{bmatrix} I_\alpha \\ I_\beta \end{bmatrix} = \begin{bmatrix} I_a \\ \frac{2}{\sqrt{3}}(I_b - I_c) \end{bmatrix} \tag{10}$$

Then the stationary system is transformed to the rotating system using Park transformation:

$$\begin{bmatrix} I_d \\ I_q \end{bmatrix} = \begin{bmatrix} cos(\theta_d) & sin(\theta_d) \\ -sin(\theta_d) & cos(\theta_d) \end{bmatrix} \begin{bmatrix} I_\alpha \\ I_\beta \end{bmatrix} \tag{11}$$

Where θ_d is the d-axis angle of the rotating reference system and is aligned with the permanent magnet flux.This is illustrated in figure 3. The rotating system rotates with the speed of the rotor. From this one can derive the d- and q-axis variables for the 3-phase synchronous machine without losses given by equations 12.

$$\begin{aligned} V_s &= \omega\sqrt{\Psi_q^2 + \Psi_d^2} \\ \Psi_q &= \Psi_{mq} + L_q \cdot I_q + L_{qd} \cdot I_d \\ \Psi_d &= \Psi_{md} + L_d \cdot I_d + L_{dq} \cdot I_q \\ T &= \frac{3}{2} \cdot \frac{N_m}{2}(\Psi_d \cdot I_q - \Psi_q \cdot I_d) \end{aligned} \tag{12}$$

The subscript d and q are the d- and q-axises respectively. Ψ is the flux linkages and L is the inductance. FSCW configurations usually introduce more spacial harmonics, both the sub harmonics and over harmonics will change the shape and even shift the flux density in the air gap. The shape is considered more trapezoidal then sinusoidal. When using the Park transformation for trapezoidal air gap flux densities the model deviates significantly. This is studied in [9] where this effect reduces the motors total field weakening performance. The paper finds a reasonable solution to the problem by shifting the axis. The shifting angle is found by comparing the fundamental components between DW and CW in the specific motor.

G. Star Of Slots

By using star of slots [10] it is easy to find the winding factor and the winding angle. In this paper the winding angle is of special interest when applying the d and q-axis currents.

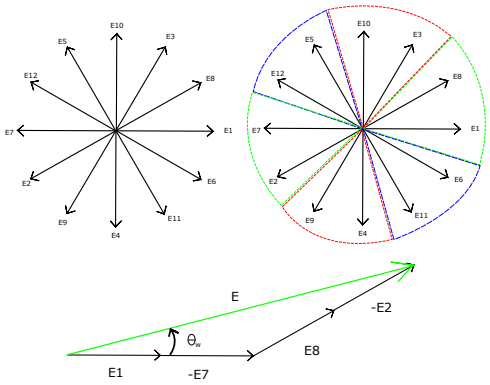

Fig. 4: Laying out the star of slots and dividing them into phasebelts of 60 degrees

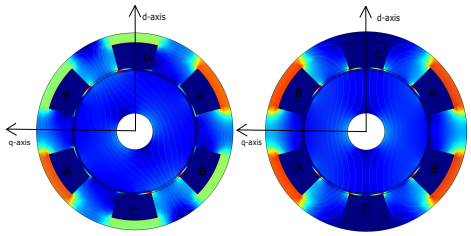

Fig. 5: 6 slot/2 pole machine. Left) current angle is zero. Right) current angle is shifted -θ_w.

The fundamental idea behind star of slots theory is to think of each slot as having equal emf but shifted in space around the stator. The angle between the slots θ_{slot} is found by 13:

$$\theta_{slot} = \frac{\pi}{N_m \cdot N_s} \tag{13}$$

The emf vector for each slot is then plotted, this is illustrated in figure 4. Then the vectors are separated by a phase belt (usually 60 degrees), which then defines the three phases A, B and C. The winding factor can be found by summing the phasors:

$$k_w = \frac{\sum E \angle \theta_E}{\sum E} \tag{14}$$

Where each stator emf has a angle θ_E and a length E. The winding angle is equal to the resulting vector and can be found by:

$$\theta_w = \arctan \frac{\sum E \sin \theta_E}{\sum E \cos \theta_E} \tag{15}$$

To apply a current in the d-axis, the current must be shifted by $-\theta_w$. This is illustrated in figure 5. The PM's are not included to give a better view of the flux lines.

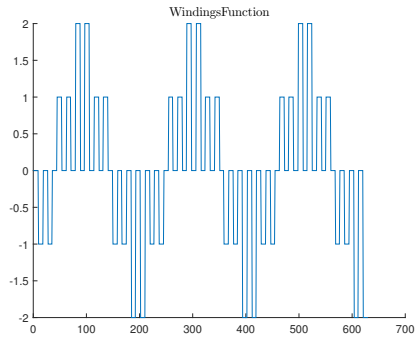

Fig. 6: Total winding function of 3 phase 72 slots and 66 poles SL.

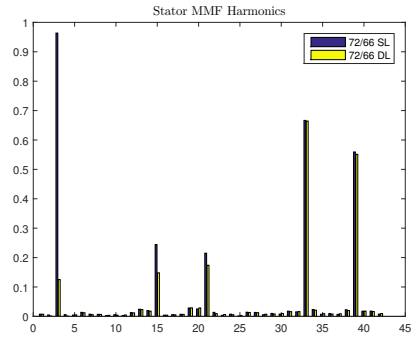

Fig. 7: The harmonic stator MMF for DL and SL.

H. Winding Function and Harmonics

After applying the star of slots method with a phase spread of 60 degrees, the 3 phases are distributed over the slots. It is then interesting to analyze the spatial stator MMF harmonics. Start by making the winding function for one phase. This is done by iterating over the slots and adding the MMF contribution for each slot. The MMF contribution depends on the slot, if it is a positive or negative phase. If the winding layout is DL the contribution is half of a single layer. It must be remembered that the winding function only depends on the winding layout around the stator and is done in mechanical degrees. When this is done for every phase the winding function is multiplied by the phase current at time zero respectively and added together. This will create the total winding function which can be Fourier transformed.

The 3 phase winding function is illustrated in figure 6 for SL. The harmonic spectrum of the winding function is shown in figure 7. The main harmonic is equal to the number of pole pairs, in this case 33. For the SL it is noticed that there are large sub harmonics, where for DL the harmonics are reduced.

I. Calculating Motor Parameters

The d-and q-axis inductance's are calculated using the flux linkage method [11]. The flux linkages Ψ_d and Ψ_q are determined by flux linkages of phase a,b and c. In a 2D FEM model the flux linkage of phase a is the difference between the average vector potential A_z in the positive phase slot S^1 and the negative phase slot S^{-1}. Summing all the phase a slots the flux linkage for phase a is :

$$\Psi_a = \sum_a \frac{1}{A_c}\left(\int_{S^+} A_z dS - \int_{S^-} A_z dS\right)\frac{N_{turns}\cdot L}{N_{par}} \tag{16}$$

Where A_c is the conductor area, N_{turns} and N_{par} is the number of turns per coil and number of parallel connections respectively. This is also equivalent for phase b and c. Using the Clark and Park transformations one can obtain the d- and q-axis flux linkage's.

1) Calculating Inductance: To find the inductance's the remanence flux density in the PM's are set to zero and the current vector is aligned to the d- and q-axises respectively. This is done by shifting the current by $-\theta_w$ and $-\theta_w + \frac{\pi}{2}$ for the d and q currents respectively. First set $I_d = I_{rated}$ and $I_q = 0$ calculated the flux linkage in d and - q-axis:

$$L_d = \frac{\Psi_d}{I_d} \quad L_{qd} = \frac{\Psi_q}{I_d} \tag{17}$$

L_{dq} and L_{qd} are the cross-saturated terms. These are usually very small but in some cases not. Then setting the $I_q = I_{rated}$ and $I_d = 0$ the q axis inductance is:

$$L_q = \frac{\Psi_q}{I_q} \quad L_{dq} = \frac{\Psi_d}{I_q} \tag{18}$$

2) Calculating PM Flux Linkage: The permanent magnet flux linkage is an important parameter in flux weakening operations. It contributes to the torque and induces voltage in the coils. This voltage is called the back emf and is proportional to the angular velocity. PM's are therefor one of the limiting factors of achieving a wide speed range.

The flux linkage is determined by turning on the PM's in the model and simulating the system without any current. The flux linkages are then calculated as described before.

J. Losses

Hysteresis losses and eddy current losses are the two main core losses in stator and rotor. During a AC cycle the current magnetizes and demagnetizes the core alternatively, resulting in moving up and down the hysteresis loop. This gives hysteresis losses (19):

$$P_h = fV_{core}\oint \mathbf{H}\,\mathbf{dB} \tag{19}$$

Where V_{core} is the volume of the core and f is the frequency. H is the magnetic field intensity and B is the magnetic flux density. The BH-curve shows the relationship between these two values. Sometime this relationship is assumed linear, then $\mathbf{B} = \mu\mathbf{H}$ where μ is material permeability and is constant. The losses are proportional to the frequency and the BH-curve is given by the material property. A typical BH-curve is shown in figure 8.

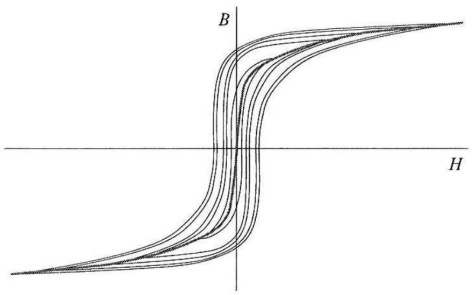

Fig. 8: Typical magnetization curve for a ferromagnetic material [7]

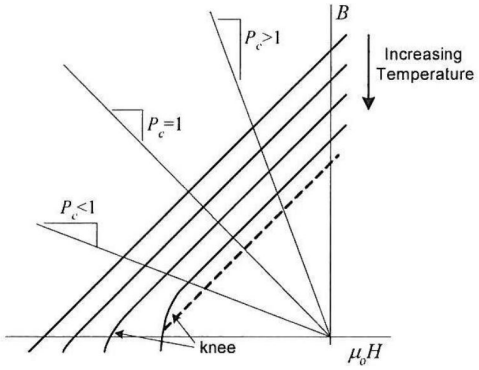

Fig. 9: Influence of temperature on the demagnetization curve [7]

Eddy currents are induced by alternating magnetic fields. The losses are then dependent on the frequency, the conductivity of the material and the magnitude of the flux density. Eddy current losses are determined by (20):

$$P_{eddy} = \iint \frac{J_z(x,y)^2}{\sigma}\, dA \tag{20}$$

Where σ is the material resistivity and J_z is the current density in the z-direction. The core losses will increase the temperature and this can demagnetize the permanent magnet (PM), illustrated in figure 9. Eddy currents are proportional to the frequency squared. It is then reasonable to assume hysteresis losses are dominant in low speed and eddy current losses dominates in high speed operations.

The rotor and stator core are usually laminated in a PMSM, which consists of dividing the metal into thin layers and then compressing them together. This is done to reduce the losses inside core. Due to the core lamination's it is difficult to calculate the core losses in a 2D FEM simulation. The most used method to calculate core losses is an estimation formula, which has been developed through the years. Some time's known as the Steinmetz or Bertotti's equation and is based on loss separation:

$$P_{loss} = k_h f B^{\alpha} + k_e f^2 B^2 + k_a f^{1.5} B^{1.5} \tag{21}$$

Where k_h,k_e and k_a is hysteresis, eddy current and excess loss coefficients. Depending on the used method these coefficients can be constant or variable with frequency and flux density. Many methods exists in calculating the coefficients, the method proposed in this paper is a curve fitting method. Steel manufacturers usually provide data from an Epstein frame test. This data gives core losses at different flux densities and frequency's, thereby giving the opportunity of curve fitting the data to the loss separation equation 21. Manufacture data is then used by quadratic fitting [12]:

$$\frac{P_{loss}}{f} = \underbrace{k_h B^{\alpha}}_{a} + \underbrace{k_a B^{1.5}}_{b}\sqrt{f} + \underbrace{k_e B^2}_{c}\sqrt{f}^2 \tag{22}$$

Depending on how many data point the manufacturer provides, the accuracy of the curve fitting method varies. It is seen that five data point's gives good approximation's. The eddy current and excess loss coefficients are easily retrieved and are independent of the frequency. However k_e and k_a vary with flux density and are therefore fitted with a third-order polynomial:

$$k_e(B) = k_{e0} + k_{e1}B + k_{e2}B^2 + k_{e3}B^3 \tag{23}$$

$$k_a(B) = k_{a0} + k_{a1}B + k_{a2}B^2 + k_{a3}B^3 \tag{24}$$

The hysteresis coefficient varies with frequency and flux density and is calculated using:

$$\log a = \log k_h + \alpha \log B \tag{25}$$

The constant $a = k_h B^{\alpha}$ can first be calculated using:

$$a = P_{loss} - k_e(B)B^2 f^2 - k_a(B)B^{1.5} f^{1.5} \tag{26}$$

Where P_{loss} is the manufacturer data and the second and third term is the estimated loss using the curve fitted values. This will decrease the numerical instability. The hysteresis coefficents and exponent α is found by linear regression of equation 25.

The loss seperation model 21 assumes sinusoidal flux densities. This is not the case for a FSCW PMSM. The flux density is therefore transformed into the frequency domain by Fourier. The core losses is then calculated for each frequency band and then summed together:

$$P_{loss} = k_h B^{\alpha} f + \sum_{n=1}^{\infty} k_{en} B_n^2 f_n^2 + \sum_{n=1}^{\infty} k_{an} B_n^{1.5} f_n^{1.5} \tag{27}$$

Where the loss coefficient from the curve fitting method is calculated for each frequency and flux density. The Hysteresis loss only depends on the main harmonic as seen in the formula.

Eddy current loss in PMs is easier to estimate because the magnets are not laminated but segmented. Segmentation of magnets are used to reduce induced eddy currents in the magnets. There exist mainly three different methods of

segmentation magnets; tangentially, radially and axially. It is possible to simulate the two first segmentations easily in a 2D FEM software. The eddy current losses in the PM's are calculated using the previous formula 20.

K. Optimal Split ratio

The split ratio $\chi = \frac{R_s}{R_{s0}}$, ratio between inner and outer stator radius, is one of the most important variables in a PMSM. The split ratio has great influence on the torque density of the machine and depends on the number of slots Q and the flux density ratio β in the air gap and stator core :

$$\beta = \frac{B_{AG}}{B_{Fe,max}} \tag{28}$$

B_{AG} is the average max flux density in the air gap and $B_{Fe,max}$ is the maximum allowed flux density in the stator core. There are of course limitations concerning losses when designing a machine, this will have influence on the split ratio. The dominating losses is usually the copper losses and many studies have found the optimal split ratio when this boundary is taken account for [13]. Both the global copper losses in the windings and the max current density is important to consider. These limitation are defined by the designer, considering the cooling system of the machine. As shown in [13] the machine torque can be written based on the total allowed copper loss (global limit) and the maximum allowed current density (local limit):

$$T_P = \sqrt{\frac{2_{SL} P_{Cu,max} \cdot A_{coil} \cdot k_{coil} \cdot L \cdot Q}{\rho_{Cu}}} \cdot B_{AG} \cdot R_s \cdot \chi \tag{29a}$$

$$T_J = \sqrt{2} \cdot Q \cdot J_{max} \cdot A_{coil} \cdot k_{coil} \cdot L \cdot B_{AG} \cdot R_s \cdot \chi \tag{29b}$$

Where the total copper losses and current density must satisfy:

$$P_{Cu} = \frac{Q}{2_{SL}} \cdot \frac{I^2}{2} \cdot \rho_{Cu} \cdot \frac{N^2 \cdot 2L}{A_{coil} \cdot k_{coil}} \tag{30a}$$

$$(N \cdot I_{rms})_{max} = J_{max} \cdot A_{coil} \cdot k_{coil} \tag{30b}$$

k_{coil} is the winding fill factor. The factor 2_{SL} is included if single layer CW, otherwise this constant is 1. The stator back yoke is assumed to be half of the stator teeth. Avoiding saturation the tooth width is assumed to be:

$$w_{tooth} = \frac{\pi R_{s0}^2 \cdot \beta}{Q} \tag{31}$$

For this paper it is interesting considering single layer and not double layer as proposed in [13]. The optimal split ratio is found for the two cases by solving $\frac{dT}{d\chi} = 0$. Where the coil area for single layer FSCW is:

$$A_{coil} = A_{slot} = \frac{A_{stator} - A_{tooth} - A_{yoke}}{Q} \tag{32}$$

At a low split ratio the slot area A_{slot} is very large, meaning that the machine can carry a lot of current for a given current density. However there is a limit to the total copper loss set by the designer. Therefore at low split ratio's the global limit of total copper losses defines the optimal split ratio. As the split ratio increases the current density increases, until it reaches the maximum allowed current density. From this point on the optimal split ratio is defined from the max current density. The two split ratio curves are shown in figure 10.

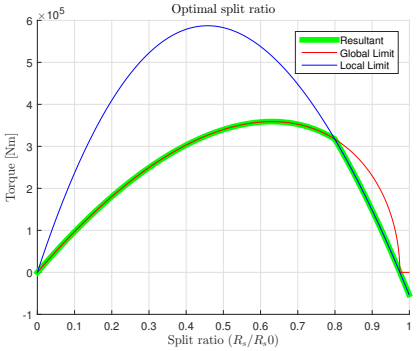

Fig. 10: Torque vs split ratio for two limitations. Global limit: Total copper loss, Local Limit: Current density. The region inside the resultant curve satisfy both global and local limitations.

Analaytical evalutaion of the optimal split ratio is used as a starting point in machine optimization. In this paper the purpose is to compare SPM to IPM FSCW machines. Since the optimal ratio is dependent on the flux density ratio β the change in split ratio must be considered. With V-shaped PM's there is the ability to change this flux ratio by varying the angle. An SPM can't be compared to an IPM without considering this. On the other side one could keep this ratio and the number of slots constant when comparing these two machines. Figure 11 and 12 shows the change on torque for increasing values of β and Q.

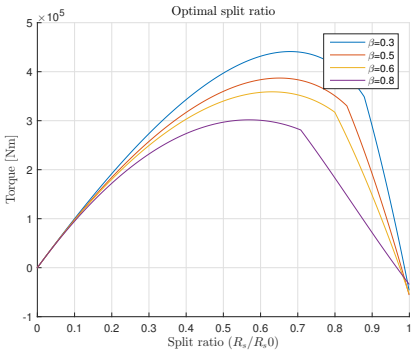

Fig. 11: Torque vs split ratio when change flux density ratio β.

Seen from figure 11 increasing β increases the optimal split ratio drastically. From figure 12 there is not much change in optimal split ratio when changing Q. However it is more realistic to change the value of air gap flux density and keeping the maximum allowed stator flux density be constant equal to

1.7 T. This is more reasonable then just changing the ratio and is showen in figure 13

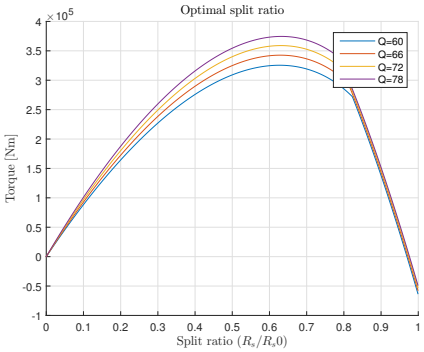

Fig. 12: Torque vs split ratio when change in number of slots Q.

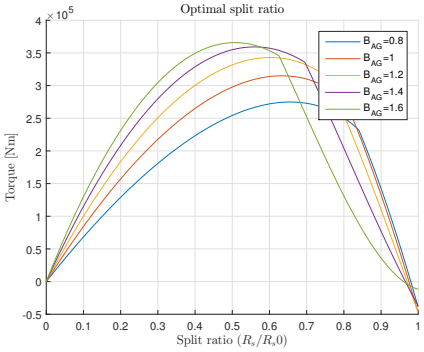

Fig. 13: Torque vs split ratio when change air gap flux density and maximum allowed core flux density is kept constant.

In figure 13 it is that when increasing air gap flux density the optimal split ratio decreases. There are many other variables one could look at concerning the optimal split ratio, this is not done here. The purpose of this section is to show a little of how important this ratio is. However the core losses must also be evaluated and is complex to do without a 2D FEM simulation of the machine. Low split ratio will also give a very large stator which also will give a big cost as well as large core losses.

III. Field Weakening Considerations

A. The Concept Of Field Weakening

A synchronous machine is usually driven by a converter. Below rated speed, the induced voltage is less then the rated voltage. If the speed goes beyond rated speed the converter will be destroyed because of the high induced voltage. To overcome this problem the machine goes into a field weakening mode. In this mode the current is shifted to the negative d-axis to reduce the flux. This is illustrated in figure 14, where γ is the current angle. This reduction makes it possible to increase the speed beyond the rated speed. Using equations 12 the stator voltage can be written as:

$$V_s = \omega\sqrt{(L_q I_q)^2 + (\Psi_m + L_d I_d)^2} \tag{33}$$

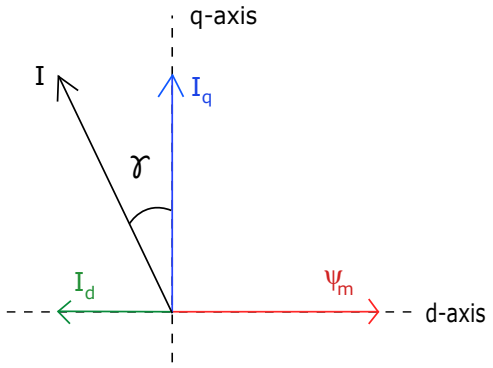

Fig. 14: d- and q-axis current when the current is shifted in the negative d-axis.

Looking at equations 33 the voltage is proportional to the speed and the flux linkages. When increasing the speed the flux linkage must be reduced to keep a constant voltage. This is done by applying negative d-axis current. Note that in flux weakening mode $L_d I_d < \Psi_m$. The produced torque can be written in a more convenient way:

$$T = \frac{3}{2}\frac{N_m}{2}(\Psi_m I_q - (L_q - L_d) I_d I_q) \tag{34}$$

Where the first term is the electromechanical torque and the last term is the reluctance torque due to the saliency in the machine. The maximum current and voltage is usually limmited by the inverter. Controlling the voltage is done by adjusting the current:

$$I_d^2 + I_q^2 = I_s^2 \leq I_{max}^2 \tag{35}$$

$$V_d^2 + V_q^2 = V_s^2 \leq V_{max}^2 \tag{36}$$

B. SPM Motor Designs

SPM machine's are usually thought to be poor in flux weakening because of their low inductance's, but many studies have proven that FSCW can have good flux weakening capabilities [3], [14]. The main reason behind this is because of the high leakage inductance due to the large harmonic spatial flux components in FSCW. Important design considerations in FSCW is the stator opening geometry. Increased inductance reduces the characteristic current (1), making it easier to achieve optimal field weakening.

Choosing the right q value (slots per pole per phase) is important when optimizing SPM for flux weakening. [1] highlights important factors when choosing q:

1) The winding factor for the fundamental frequency should be as high as possible
2) LCM(N_s,p) should be as high as possible. This number represents the cogging frequency. The higher the frequency the lower the cogging magnitude.
3) GCD(N_s,p) should be even. This number represents the periodicity. A even number gives low net radial force on the machine.
4) q must support single layer winding

[1] Concludes optimal q for FSCW is 2/5 and 2/7. It is also reviled that for the same PM flux linkage the inductance of FSCW is 6.56 times larger then for a DW, assuming sinusoidal flux density. Subsequently it is much easier to reach the optimal flux weakening region, because of the reduced characteristic current (1). The reason behind choosing single layer winding is that the subharmonic flux density components are larger then for double layer windings. This gives important contributions to the leakage inductance and also reduces the characteristic current.

CW have many significant advantages over DW. Shorter end turns which reduces copper volume, losses and the total axial length of the machine. CW has high reliability and compatible with segmented stator which makes it possible to achieve much higher fill factors [1].

C. IPM Motor Designs

IPMs have two flux weakening parameters; saliency ratio (3) and characteristic current (1). DW tend to have better field weakening capabilities compared to CW in IPM machines. This is mainly because CW have very small mutual inductance between phases, subsequently the saliency ratio is much higher for DW then CW IPM's.

A significant advantage high salient IPM motors have over non-salient motors is the low back emf induced voltage. At high speeds, in case of an inverter failure, the back emf can be limited so that the inverter isn't destroyed. In non-salient machines the magnets are the only contribution to torque, so the magnets need to be strong. In salient pole machines reluctance torque is also a contribution, and the magnets can be weaker. IPM machines can also be expected to have higher torque in the field weakening region if the machine have high saliency.

Increased saliency ratio will give a larger reluctance torque and hence, the PM flux linkage can be reduced. This will yield a wider flux weakening capability and more torque in the flux weakening region. DW will therefore have an advantage over FSCW in field weakening.

Optimizing a IPM machine for field weakening can be done two ways. Either increasing the saliency ratio or making the characteristic current equal to the rated current. This kind of rotor gives also more creative possibilities of magnet shape and flux barriers. It is observed that V-shaped magnets can increase the PM flux linkage when the correct angle is chosen.

1) Flux Barriers: Flux barriers are used to avoid short circuiting of the PM's and manipulate the magnitization profile. These barriers can be used to increase saliency and reduce torque ripple of the IPM [15].

One interesting design proposed in [16] takes the advantage of iron bridges between the magnets (figure 15), this advantage increases the flux weakening capability. The negative d-axis current has two jobs. 1) When negative d-axis current is applied, the air gap flux linkage is reduced. 2) Additionally the PM leakage flux in the bridges are increasingly canceled by the negative d-axis current. This gives room for more flux in the bridges from the PM leakage. Resulting in even less PM flux linkage in the d-axis.

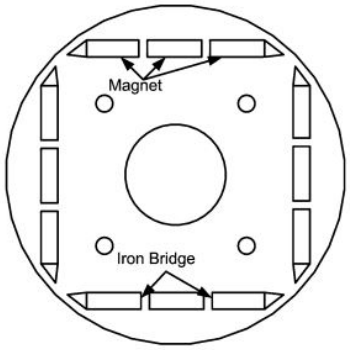

Fig. 15: IPM segmented magnets with 2 iron bridges in the d-axis flux path [16]

2) Saliency ratio: There are two different saliency ratio's to consider in a IPM; saturated and unsaturated. The unsaturated saliency is the maximum saliency the machine can achieve. However at rated conditions the machine usually operates with saturation, because of high currents. The saliency ratio depends on the amount of current, and usually decreases with increasing current. The two different parameteres must be considered when designing a IPM. The unsaturated and saturated saliency ratio's can be expressed as 37

$$\begin{aligned} \xi_{unsat} &= \left.\frac{L_q}{L_d}\right|_{I\approx 0} \\ \xi_{sat} &= \left.\frac{L_q}{L_d}\right|_{I=I_{rated}} \end{aligned} \tag{37}$$

3) Characteristic Current: As mentioned above due to saturation inductance values change non-linearly. This also influences the characteristic current in IPM's. When saturation is accounted for the characteristic current is defined as the current which the d-axis flux linkage is zero. So to get this value one must measure the d-axis flux linkage with the PM's turned on and while increasing the negative d-axis current. When the flux linkage is zero in the d-axis, the characteristic current is found. This concept is mentioned in [6].

D. High Speed Losses

FSCW SPM machines are very fragile when it comes to eddy current losses at high speed. This is because of the high flux density in the air gap combined with the spatial harmonics. IPM's however are shielded by the rotor iron and resulting in less eddy currents induced. Sub harmonics and over harmonics rotating at different speeds then the synchronous, contributes to large alternating fields seen by the rotor. Sub harmonics cause extra saturation in the stator increasing hysteresis loss. Some harmonics rotate apposite of the rotor reference direction if this is a sub harmonic the eddy current losses in the rotor will increase. Therefore it is important to concider eddy current losses in FSCW.

The air gap often acts like a low pass filter [17]. Therefore the subharmonics and the first slot harmonics are dominant when it comes to rotor losses. In general the slot harmonics have considerable impact on the eddy current losses.

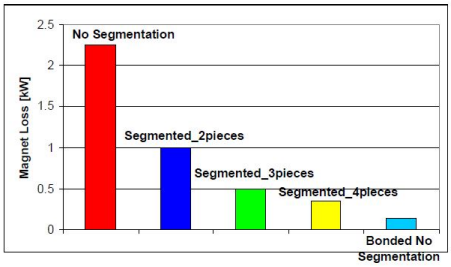

Fig. 16: Effect of segmentation and using bonded magnets on reducing the magnet losses at 6000 rpm for the 36 slot/ 42 pole design [19]

Bonded magnets can be used to reduce eddy currents because of their high inner resistance, but they have much lower remenance flux density. In [3] it was designed a optimal flux weakening motor with bonded magnets. The bonded magnets had an inner resistance of $20\mu\Omega m$ compared to sintered magnets with resistance of $0.5 - 1.5\mu\Omega m$. In figure 16 the effect of segmentation and use of bonded magnets are compared for a FSCW SPMSM. For bonded magnets, low remenance flux density increases the size of the magnets and the inertia of the rotor becomes higher. This leads to reduced dynamic performance. Therefore SPM machines should rather use segmented PMs, because they need the high flux linkage from the PMs to produce torque.

In IPM's however bonded magnets can be utilized because of the added reluctance torque the saliency ratio produces. This gives much less eddy current losses at high speeds in the magnets. The limiting factor in achieving high speeds using field weakening is losses and the loss of torque.

In [18] the performance of FSCW and ISDW IPMSM where compared. The results show that the eddy current losses at high speed are much larger for the FSCW. However for the DW the core losses and also copper losses are much higher. It was not used bonded magnets in the rotor, which could drastically improve the eddy current losses for the FSCW IPM. [6] Also gives a good in depth compare of the FSCW and ISDW IPMSM. The paper concludes that choosing between FSCW and ISDW depends on what the key feature of the machine should be. ISDW has low rotor losses at high speeds and FSCW have high efficiency at high speeds.

E. Variable Flux Machines

The use of low coercive force magnets have many interesting possibilities achieving high efficiency across a wide speed range. Magnets like AlNiCo have the ability to reduce and increase its remanent flux density. When applying a d-axis current pulse, either positive or negative, depending on the purpose, the remanent flux density is changed. The disadvantage of this kind of machine is that low coercive force magnets are easily irreversible demagnetized, but can easily be fixed by designing the machine to able to re-magnetize them at all times. The torque density will be lower then for PM-machines with NdFeB, many studies have been done on hybrid solutions [20]. Hybrid VF-machines use AlNiCo and NdFeB Magnets, but still the torque density is lower.

Today's machines are designed so the magnets are never demagnetized at the highest operating temperature. When increasing the rotor speed the induced voltage will increase linearly. Reaching the maximum voltage, which is limited by the converter, field weakening must be introduced. Field weakening will shift the armature current to the negative d-axis. This will then induce a magnetic field working against the PM magnetic field and hence weaken the field. This gives the ability to increase the speed.

Instead of field weakening, the use of VF machines can be implemented. Applying the d-axis pulses will reduce the field instead of constantly applying negative d-axis current. This will reduce copper losses and core losses in the machine achieving higher efficiency across higher speed ranges.

IV. Preparing FEM Model

COMSOL Multiphysics 5.2 is the tool used to analyse the different machines. Recently an application, simulating rotating machines, was made [21]. This application makes it easy to analyze different types of machines fast. The application lets you specify all the machine parameters and creates a model. This model can then be used to analyse the machine. However some limitation is found in the application for analyzing field weakening performance.

The application has therefore been extended for the use and study considering field weakening. Extensions made to the application is:

1) Extend Geometry
   a) Add slot opening
   b) V- and I-shaped IPM
   c) Flux Barriers
2) Compute Field Weakening Curves
   a) Torque vs Speed
   b) Power vs Speed
3) Eddy current losses in PM's
4) Iron saturation using BH-curve
5) Analyse of inductance's and flux linkages using above theory from section II-I

As mentioned in section III-B the slot leakage inductance is dominant in FSCW. To properly model these types of machines slot openings where include, which are important for the slot leakage. Flux barriers can force the flux from the PM's over the air gap, and where added to give more futures to the IPM. The geometry of the flux barriers are important when it comes to torque ripple, THD and saliency. Also iron saturation is important to include to properly model IPMs. Some different possibilities of IPM are shown in figure 17. In this paper mainly the V-shaped and tangentially magnetized I-Shaped IPM will be studied.

A. Field Weakening Curve

The process behind computing the field weakening curves (torque and power) starts with; Step 1) computing the key parameters (inductance, PM flux linkage) with 3 stationary studies of the machine. Step 2) Based on these values and dq-theory the current angle for the maximum torque is computed by iterating from 0 to π with an accuracy based on the

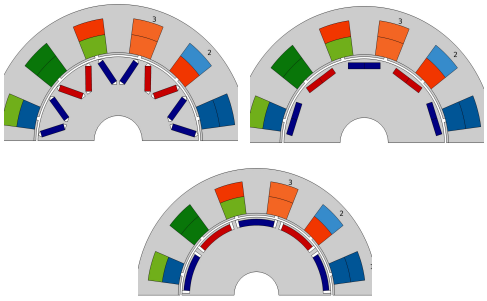

Fig. 17: Types of IPM

precision. Step 3) Based on the input of rated speed or rated voltage the maximum speed and angle is calculated with dq-theory. Here the iteration is between rated torque T_{rated} and one tenth of the rated torque $\frac{T_{rated}}{10}$.

Step 2 and 3 is only based on theory and does not include non linear behavior. These steps only provide a fast way to predict the performance. To get more accurate values one can load field weakening study and choose compute. This initiates a parametric stationary study in COMSOL, where torque and power is computed for different current angles. The theoretical maximum speed of one step can be calculated using the calculated d and q axis flux linkages using equations 12:

$$\omega = \frac{V_{rated}}{\sqrt{\Psi_d^2 + \Psi_q^2}} \tag{38}$$

This will then keap the voltage equal to the rated voltage at all speeds. The predicted power is calculated using $P = T\omega$. It is also convenient to plot the torque and power as a function of speed [rpm]:

$$N[rpm] = \omega \frac{60}{\frac{N_m}{2} \cdot 2\pi} \tag{39}$$

B. Losses

1) Post processing: Livelink with Matlab was used to post-process the mesh data after a time simulation in COMSOL. The method used is proposed by Lagerström [22]. For each model the Matlab code would open the model (mphopen) and fetch the flux density data from the solution (mpheval). It is important to specify the pattern as gauss to avoid getting several points from each mesh element. To calculate the losses the area of each mesh element is also needed, this can be obtained by the variable dvol. Dvol is a volume factor and together with the mesh type the area can be calculated. The mesh type can be a triangle, tetrahedron, prism, pyramid identified by the values 3,4,6,9 respectively. Each mesh type has a scaling number (triangle = $\frac{1}{2}$, tetrahedron = $\frac{1}{3}$, prism=$\frac{1}{6}$, pyramid = $\frac{1}{2}$) which you multiply with dvol to get the area:

$$A = meshtype \cdot dvol \tag{40}$$

2) Processing each element: Before applying a fast Fourier transform using the built in function in Matlab, the flux density reference angle should be considered. The before and after scaling of an mesh element is shown in figure 18.

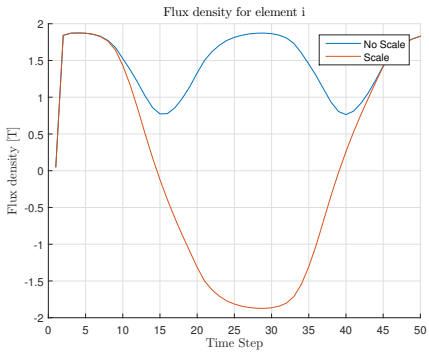

Fig. 18: Impact on the flux density when scaling after finding reference angle

For each element the reference direction is calculated by finding the maximum absolute value of the flux density over the time period. The angle of the flux density at this time is assumed to be the reference angle. Seen from figure 18 a Fourier transform of the non-scaled flux density would cause a big error. After the fast Fourier transform is applied the loss of each frequency and amplitude is summed up and added to the total core loss of the domain. The algorithm is shown in figure 19.

Using fast Fourier transform the frequency bins are separated by F_s/n, where F_s is the sampling frequency and n is the length of the signal.

Including eddy currents in the model is done by adding a single turn coil to the permanent magnets and assigning the current to be zero. In this way the sum of the eddy currents will be zero at all times in the simulation. Of course the PM's conductivity must be set the desired value. Then in post-processing one can calculate the losses in the magnets by integrating over them and using above theory.

3) Validation: The model used to calculate core losses does not include:

1) Minor hysteresis loops
2) DC-bias

The reason for not including this is that the calculations will be more complicated and more time consuming. It is shown that the DC-bias and minor hysteresis loops increase the hysteresis losses [23] [24]. Because of this the model accuracy is slightly reduced and one can assume higher losses. In the case of this paper the estimated losses are used to compare machines, and the model holds for this purpose.

4) Curve fitting: The proposed curve fitting method was used to fit the manufacture core loss data from the Epstein frame test to the loss separation model. The steel lamination data of M400 50A was used [25]. The curve fitted values compared to the manufacturer data is shown in figure 20. The figure shows that the curve fitted values corrspond well with the manufacturer data.

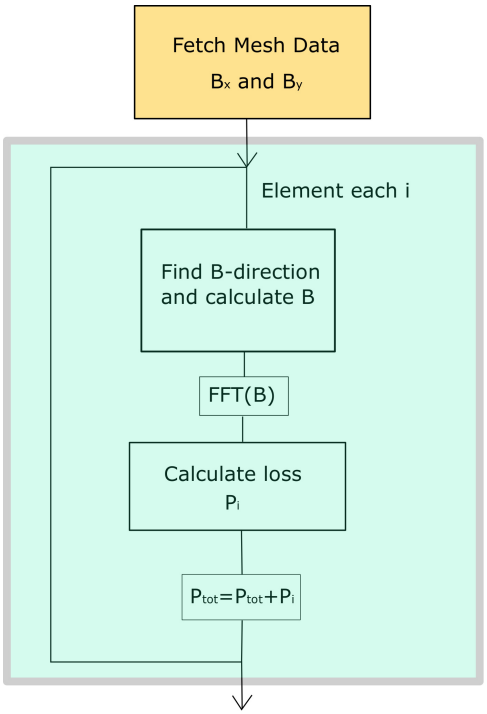

Fig. 19: Block diagram illustrating the steps to calculating total losses from the mesh data

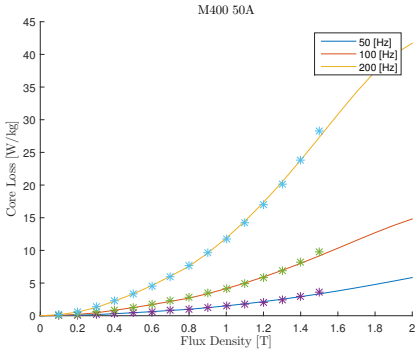

Fig. 20: Manufacturer data and curve fitted values for 3 different frequencies

The third order polynomials for the eddy current and excess loss coefficients together with the values of hysteresis coefficient and exponent are passed on into the loss algorithm. Depending on the frequency and flux density the loss is calculated for each mesh element in the model.

$$k_e(B) = (9.82 - 31.26B + 46.37B^2 - 14.7B^3)10^{-5} \quad (41)$$

$$k_a(B) = (0.7304 + 5.962B - 6.443B^2 + 1.64B^3)10^{-3} \quad (42)$$

Since the manufacturer data only has measurements up to 2 Tesla, the model does not hold for higher values. Flux densities above this value uses the coefficients at 2 Tesla. The loss coeficient for hysteresis loss is shown in table I and the third order polynomials eddy and excess loss coefiecients are given in equation 41 and 42. The Matlab code for the loss calculation and curve fitting is shown in appendix A.

TABLE I: Hysteresis Loss Coefficients for M400 50

Induction $[T]$	Frequency [Hz]	k_h [W/kg/Hz/T^α]	α [-]
$B < 0.4$	50	0.0325	2.88
	100	0.0236	2.82
	200	0.0259	2.83
	400	0.0253	2.83
	1000	0.223	2.79
$0.4 < B < 0.8$	50	0.001	1.76
	100	0.010	1.65
	200	0.010	1.66
	400	0.010	1.67
	1000	0.011	1.74
$B > 0.8$	50	0.012	2.88
	100	0.012	2.82
	200	0.012	2.83
	400	0.012	2.83
	1000	0.12	2.79

C. Convergence Issues

When using time dependent solver in COMSOL there will problems converging. This problem increases when nonlinear features are included in the model. This can for instance be iron saturation, induced eddy currents and more complex geometry. Solutions to these problem includes changing material parameter's and solver settings.

From experience convergence issues are more present with v-shaped IPMs when including eddy currents and saturation. It is not sufficient to only include conductivity to the PM's. Setting air conductivity to 10 S/m and iron to 10 S/m helps convergence. In solver settings change, under time dependent solver→time steps taken by solver, to strict and time dependent solver→Error estimation to exclude algebraic. This also helps when convergence is an issue. However when using the strict solver errors will emerge since the solver is forced to only compute results at the set time steps. Using the free solver the time simulation is free to control the step size based on the error, this will give a better solution. The strict solver should therefor only be used when the free solver does not converge or uses a very long simulation time. For this paper the strict solver is only used to estimate the eddy current losses in the PMs. All other variables are calculated using the free solver.

Meshing is also critical when attaining an accurate solution and convergence. Sharp corners should use the future corner refinement. There is always a balance between convergence and meshing. If the meshing is too fine the solution will be time consuming if the mesh is to coarse the solution will not converge. Finding this balance is difficult and comes with experience. Other methods of increasing convergence in time simulations is changing the initial rotor position and applying a stationary step before time-dependent.

V. Machine Parameters

A FSCW SPM machine will be the reference machine when comparing to the IPM machines. The stator dimensions

TABLE II: Main dimensions of 72 slot/66 pole SPM machine.

Active length [mm]	770
Outer radius [mm]	950
Rated Current [A]	1340
Rated Voltage [V]	690
Rated Speed [rpm]	75

TABLE III: SPM machine performance

Machine	T_{avg} [kNm]	T_{ripple} [%]	V_{peak} [V]	PF [-]	THD [%]
75 [rpm]	153.4	1.07	566	0.82	8.73
250 [rpm]	51.64	1.99	587	0.90	13.55

and rated values will be held constant for all machines. The key parameter's are shown in table II.

The goal of this paper is to compare the SPM to different variant of IPM and discuss which type is optimal for field weakening. The remenant flux density is set to 1.2 T and the conductivity of the magnets are set to 0.67 MS/m. The stator dimensions are kept constant and only the rotor is changed. The radially magnetized I-shaped rotor was not considered because it was not able to reach the rated torque without having a very high torque ripple.

The outer rotor radius of the IPMs is adjusted to be where the outer radius of the SPM plus 1 mm. The extra 1 mm is because the SPM machine has a small protection layer so that the magnets won't fall off at high speeds. The IPM machine doesn't need this.

VI. SPM Performance

The SPM is used as a reference for the other machine designs in this paper. The machine performance is shown i table III. The SPM is simulated with one segmentation in the magnets so it is easily compared to the V-shaped IPM design.

The d and q axis inductance is 0.70 mH and FWI is 1.25 for the SPM machine. The loss at 75 rpm and 250 rpm is shown in figure 21 and the torque and speed curve is shown in figure 22.

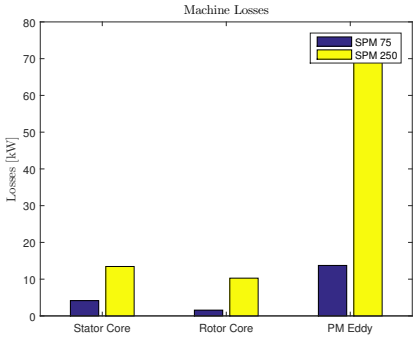

Fig. 21: Estimated loss for the SPM reference machine

It is clear that the PM loss is the dominating loss in the machine and is a big limitation when it comes to field weakening range. The torque drops fast as the speed increases which also restricts the range. The magnet flux linkage is measured to be 1668 mWb and optimal field weakening can be achieved by increasing the d-axis inductance or reduce the PM flux linkage. Reducing the flux linkage will reduce the peak torque at rated speed which is not desirable. On the other side increasing the d-axis inductance will reduce the PF and increase the cost of the converter.

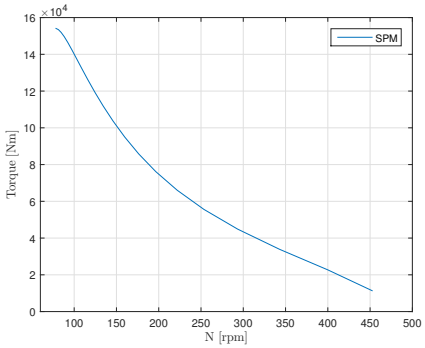

Fig. 22: Torque vs speed curve for the SPM machine

TABLE IV: Parameters for Case 1-5. Rotor Yoke and IPM depth is held constant.

Parameter	Case 1	Case 2	Case 3	Case 4	Case 5
a [mm]	2	2	2	2	5
b [mm]	5	5	1	1	1
c [deg]	0	50	0	0	0
δ [deg]	55	55	60	55	40
PM area [mm^2]	1296	1296	1224	1296	1452

VII. Optimizing V-Shaped IPM

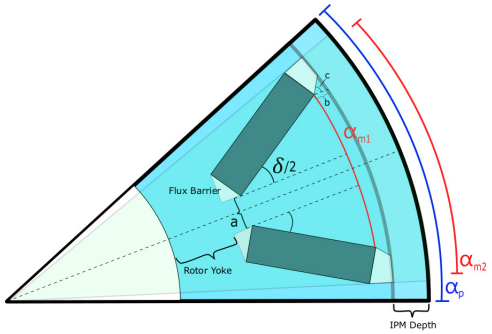

Fig. 23: V-Shaped IPM Layout.

In figure 23 the rotor geometry of the V-shaped IPM is illustrated. When optimizing the IPM the outer magnet pitch α_{m2} and IPM depth is held constant at 0.92 and 1 mm respectively. The magnet space a, magnet angle δ and top flux barrier height b and angle c will be analyzed. The V-shaped magnets have the ability to focus the flux between them, this increases the flux linkage in the winding.

The V-shaped IPM has many parameters which can be changed. Each parameter affect different variables as PM flux

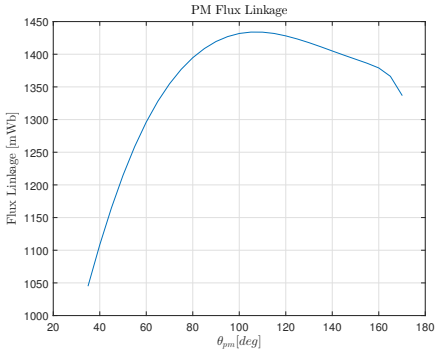

Fig. 24: Magnet flux linkage when variation in PM angle δ

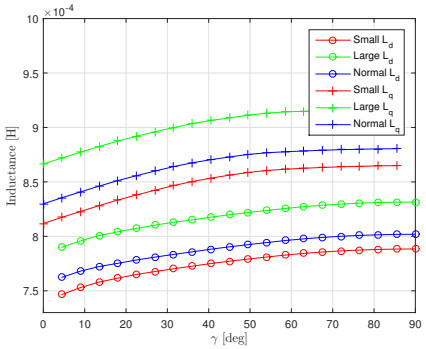

Fig. 25: d- and q-axis inductance when varying the rotor yoke length.

linkage and inductance. It is therefore important to be aware of this. Some of these parameters are now discussed.

1) PM angle (δ): From figure 24 it is seen that the maximum flux linkage per magnet volume accrues at approximately 110 degrees. However the pole pitch, defined by the number of poles, restricts the total size of the magnet. This makes it impossible to reach a high PM flux linkage at this angle. Reducing the angle gives more space deeper inside the rotor, making it possible to achieve a high flux linkage. It is observed that angles between 30-65 has the ability to produce the same PM flux linkage as the SPM.

2) PM space length (a): Increasing the space length between the magnets increases leakage flux. It is seen that the flux linkage is reduced linearly with the space length. Therefore the magnets needs to be larger to achieve the same flux linkage. However it is also observed that the increase in space length also increases the d-axis inductance.

3) Rotor Yoke: Changing the rotor yoke length can change the saturation level in the yoke and bridge between the magnets. This can be used to adjust the d- and q- axis inductance and is illustrated in figure 25. A small yoke leads to high saturation, this will help block the path of sub harmonic flux lines (the long lines). Since the sub harmonics increase the inductance, increasing the saturation will reduce the inductance. Since the machine is design for optimal field weakening the rotor yoke is adjusted accordingly. From figure 25 it seen that the d- and q-axis inductance increases as the current angle increases. As the q-axis current is reduced the saturation in the rotor is also reduced. This will increases the inductance. A large rotor yoke also increases the saliency slightly.

4) Performance: Five different machines, where d-axis inductance is adjusted for optimal flux weakening, rated performance and performance in field weakening will be evaluated. The rotor parameters are shown in table IV. Since there is many parameters one can change in the rotor geometry, it will be very time consuming to analyze each and every parameter separately. Because of this five cases are compared with different rotor geometry. Results are shown in table V. Seen from the table it is clear that small adjustments in the rotor has huge impact on the performance. Case 1-and 2 shows the difference when increasing the flux barrier angle c. The PM leakage flux increases which leads to a smaller average torque, the torque ripple is reduced in field weakening and the peak

TABLE V: Results from time simulation at 75 and 250 rpm of Case 1-5. Current angle γ =20 deg and γ =70 deg.

Variable	Case 1	Case 2	Case 3	Case 4	Case 5
T_{avg} [kNm]	149.09	145.85	151.28	155.12	155.27
	58.42	56.69	59.33	60.61	60.26
T_{ripple} [%]	0.75	1.05	0.57	0.85	1.03
	2.51	1.25	2.06	3.03	3.04
V_{peak} [V]	596	585	595	598	563
	621	597	617	624	625
THD [%]	13.32	13.16	14.03	13.36	9.70
	13.58	13.70	13.90	12.98	11.66
PM Loss [kW]	8.80	8.65	8.54	9.54	12.07
	58.4	60.1	57.1	60.6	71.0
PM Loss [W/mm^2]	6.8	6.7	7.0	7.4	8
	45	46	47	47	49

phase voltage is reduced. From this it is clear that an optimal angle exists. From case 4 and 3 the PM angle is reduced from 55 degrees to 60 degrees. This reduces the torque ripple and the loss, but the average torque is reduced. Case 1 and 4 the flux barrier length b is reduced. This increases the losses, torque ripple but increases the torque. In the last case the space length a between the magnets is increased. This leads to much more loss and much higher THD in field weakening. However the peak phase voltage is lower then all the other cases.

To achieve best possible performance in field weakening some observation are made. The PM angle should be as high as possible to reduce torque ripple. Increasing the space length a reduces the THD but leads to higher PM leakage flux which increases the PM material. Increasing the flux barrier height b the PM losses and torque ripple is reduced. It was also discovered that increasing the PM height reduced the PM losses significantly, but increases the torque ripple.

A. Slot per Phase per Pole (q)

The influence of changing the pole number is considered. In table VI the winding factor, LCD and symmetry is given for different pole numbers. When choosing SPP the symmetry should be high to avoid long simulation time, LCD should be high to reduce the cogging torque and lastly the winding factor should also be high.

Increasing number of poles leads to reducing flux per pole

TABLE VI: Winding factor, LCD and symmetry for different pole combinations for 72 slots SL.

Poles	56	60	64	66	68	76	78	80	84
K_w	0.902	0.966	0.945	0.957	0.956	0.956	0.957	0.945	0.966
LCD	504	360	576	792	1224	1368	936	720	504
Sym	4	12	4	6	4	4	6	4	12

TABLE VII: Comparison of double and single layer V-shaped IPM, 75 and 250 rpm.

Variable	SL	DL
T_{avg} [kNm]	149.09	153.41
	58.42	58.55
T_{ripple} [%]	0.75	0.57
	2.51	1.83
V_{peak} [V]	596	560
	621	628
THD [%]	13.32	6.67
	13.58	15.98
PM Loss [kW]	8.80	8.45
	58.4	36.9

and the rotor/stator yoke can be shortened. Disadvantages of high pole numbers are firstly the cost of the converter increases because the switching must be faster. The higher frequency will also increase the iron losses due to eddy currents and hysteresis losses. This should be considered when evaluating.

B. Double Layer Windings

Case 1 is further studied when changing to DL winding. When changing from SL to DL the sub harmonic spatial flux component is reduced. This will reduce the inductance in the machine. The saliency however will be increased. The V-shaped IPM case 1 was changed to DL windings holding everything else constant.

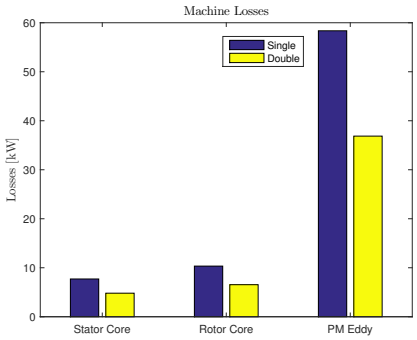

Fig. 26: Losses at 250 rpm for double and single layer winding configuration with same V-shaped rotor geometry.

From figure 26 and table VII it is clear that changing to DL winding increases the field weakening performance drastically. One exception is for the THD which increases much more then the single layer when applying negative d-axis inductance. Another factor is that for DL winding the d-axis inductance is no longer optimal for field weakening. This can be adjusted by reducing the magnet height and increasing the magnet width.

Next the saliency of the DL winding machine will be analized. The d- and q-axis inductance is measured when changing the pole number. Only the PM width is changed when varying the pole number to keep the magnet pitch constant. The results are shown in figure 27. It is seen that reducing the number of poles the d-axis inductance is reduced and hence the saliency is improved. The saliency reaches only a value of 1.1 which does not aid much in field weakening.

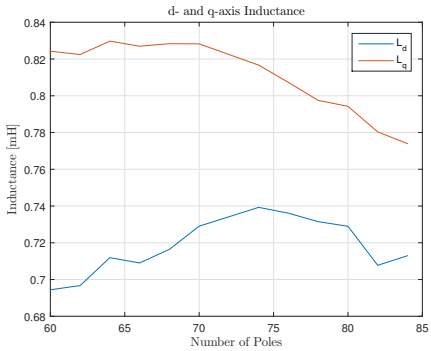

Fig. 27: Varitation in d- and q- axis inductance when changing pole number

From this it is clear that DL FSCW V-shaped IPM do not have high saliency. Instead the optimal SPP value has a large d-axis inductance. Seen from the figure the d-axis inductance is largest for 74 poles.

VIII. Optimizing I-shaped IPM

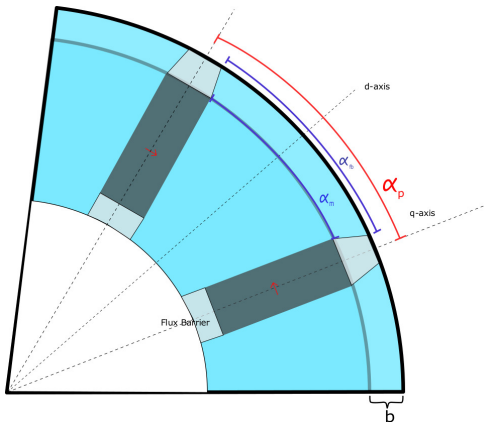

Fig. 28: I-Shaped IPM Layout.

When changing to tangential magnetized I-shaped PMs the d- and q-axis are reversed. The rotor geometry of the I-shaped IPM is illustrated in figure 28. The magnet height can be changed to adjust the inductance as well as the PM flux linkage. In this analyses the magnet height is equal to the magnets in the SPM machine. The rotor inner radius is constant for all simulations only the top flux barrier dimensions are changed. The height of the magnets are adjusted to achieve the necessary torque at rated speed of approximately 150 kNm.

TABLE VIII: I-shaped: Results from time simulation at 75 and 250 rpm of when changing top flux barrier height b. Current angle γ =0 deg and γ =70 deg.

Variable	5 mm	10 mm	20 mm
T_{avg} [kNm]	149.72	149.44	148.97
	53.89	53.73	53.59
T_{ripple} [%]	0.74	0.74	0.76
	2.72	2.67	2.71
V_{peak} [V]	621	619	618
	495	494	494
THD [%]	6.47	6.44	6.15
	9.52	9.16	9.12
PM Loss [kW]	2.78	2.62	2.52
	21.46	20.31	19.72

A. *Flux barrier height (b)*

The top flux barrier height b is changed to evaluate the flux weakening and rated condition performance. When increasing b the bottom flux barrier will be reduced since the rotor inner radius is held constant. The flux barrier pitch is held constant equal to the magnet pitch ($\alpha_{fb} = \alpha_m$). The results are shown in table VIII. It can be seen when increasing the height of the top flux barrier only has small impact on the performance.

B. *Flux barrier pitch (α_{fb})*

The flux barrier pitch (α_{fb}) is changed for when b =10 mm to minimize the torque ripple in field weakening. It is observed from figure 29 that increasing the flux barrier pitch beyond the magnet pitch will reduce torque ripple in field weakening. When increasing the top flux barrier width the inductance and PM losses increase. This will lead to reducing the field weakening capability. The flux barriers can be fine tuned for optimal performance based on the requirements.

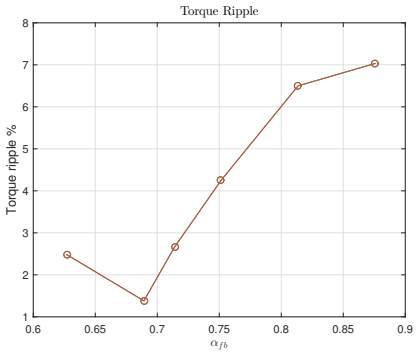

Fig. 29: Torque ripple in field weakening (250 rpm) when varying flux barrier pitch α_{fb} for the I shaped IPM. b = 10 mm and $\alpha_m = 0.75$

IX. Comparing IPM and SPM

It is a difficult task to compare the SPM machine to the two different IPM machines. Both IPM machines have a large q-axis inductance. This means that the phase voltage at rated speed, when γ=0, is much larger then for the SPM. This will increase the cost of the converter and is not desirable. One solution to this problem is to design the IPM machines to have a lower rated speed, but with higher torque. Since both IPM

TABLE IX: Machine variables

Variable	SPM	V-IPM	I-IPM	V-IPM 1
Ψ_m [mWb]	1668	1678	1674	1679
L_q [mH]	0.70	0.88	0.9	0.73
L_d [mH]	0.70	0.88	0.87	0.70
FWI	1.25	1	1	1.27
PM area [m^2]	0.0189	0.0158	0.0154	0.0142

TABLE X: Results from time simulation at 75 and 250 rpm for single layer. Where the current angle γ is approximately 0 and 70 degrees.

Variable	SPM	V-IPM	I-IPM	V-IPM 1
T_{avg} [kNm]	153	153	152	155
	52	57	54	57
T_{ripple} [%]	1.07	0.68	0.68	2.40
	1.99	2.05	1.47	7.62
V_{line} [V]	645	707	697	655
	641	654	617	693
THD [%]	8.7	10.14	5.75	9.15
	13.5	13.42	7.64	12.27
PF	0.82	0.75	0.76	0.81
	0.89	0.98	0.99	0.92
PM Loss [kW/m^2]	158	167	37	100
	849	920	273	409

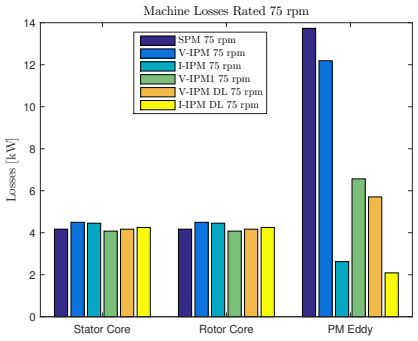

Fig. 30: Losses at 75 rpm

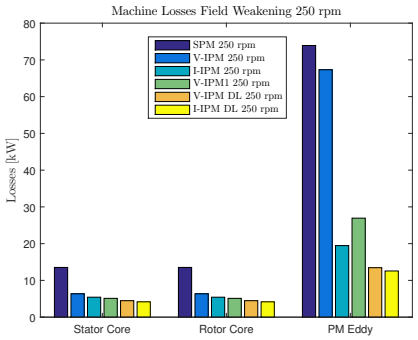

Fig. 31: Losses at 250 rpm

machines can have a high d-axis inductance achieving optimal field weakening is possible for higher PM flux linkages. Another issue with the IPM is that the high q-axis inductance reduces the power factor, this will also increase the cost of the converter.

Three single layer IPM machines are compared to the SPM machine, the parameters are given in table IX. The V-IPM and I-IPM where designed based on the results from the previous section of optimizing. The V-IPM 1 has no rotor yoke and much thicker magnets, designed to have much less loss then the other V-IPM, inspired by **??**. The results from the time simulation is shown in table X.

A. Torque

The torque and speed curve is shown in figure 32. Seen from the figure the IPMs have a longer torque curve. This is because the d-axis inductance is adjusted for optimal field weakening. However the machines must go into field weakening earlier because of the high q-axis inductance which increases the line voltage.

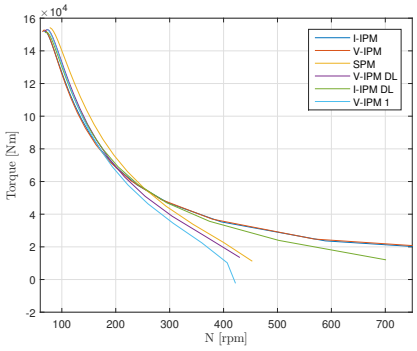

Fig. 32: Field weakening curve for all machines

The torque ripple, seen from table X, is highest for the V-IPM 1. This is caused mostly by the thicker magnets, however the losses in the magnets are reduced significantly by increasing the magnet thickness.

B. Losses

The I-shaped IPM is superior concerning PM eddy current losses. One would think that the core losses in the rotor and stator would increase accordingly, but this is not the case. The I-shaped magnets block the sub harmonic MMF in the rotor. At rated speeds this does not have an impact but in field weakening these sub harmonic MMF increase losses in both rotor and stator. The sub harmonic MMF is largest for the SPM since it does not have any flux barriers which reduce this effect.

Inserting flux barriers for the SPM in the rotor would reduce losses, but at the same time reduce the d-axis inductance, which is not desirable concerning field weakening. The IPM machines are not dependent of the sub harmonic MMF to achieve high d-axis inductance.

C. Voltage

The IPM machines have both very high q-axis inductance. This leads to a very high phase voltage at rated conditions. The high inductance also reduces the power factor at rated speed. The PF can be estimated in dq-frame as:

$$PF = \cos\left(\gamma - \arctan\frac{\Psi_q}{\Psi_d}\right) \tag{43}$$

For SPM machine the q-axis inductance is adjusted so that the flux in the q-axis is smaller then the PM flux linkage at rated speed. This will give the best PF at rated speed.

The converter will therefore be more expensive for a lower PF. In field weakening the case is different, the PF is higher and the voltage is lower for the I-shaped IPM.

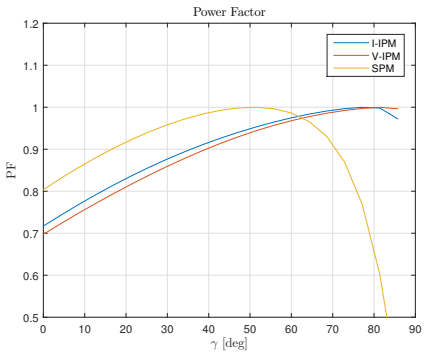

Fig. 33: Power factor as a function of the current angle γ

Figure 33 shows the estimated PF for different current angles γ. When the current angle is approximately 20 degrees the PF for the IPMs are equal to the SPM. It is clear from this that when achieving optimal flux weakening the power factor will be reduced. To achieve the highest efficiency in both converter and machine it is important to not have to high inductance. It will be waste full to design a machine for optimal field weakening, but not being able to reach the desired speed because of to much loss.

D. Double layer

It is interesting to view the effect of changing to double layer. The machine parameters and results are shown in table XI and XII. From the results it seen that the torque ripple and losses are reduced. The V-IPM is still struggling with high torque ripple and THD in field weakening. The I-IPM with DL still has a decent torque/speed curve in field weakening and the PF is just below 0.8. However DL windings are known to have a lower fill factor then SL.

X. Discussion

Overall the IPM machines have reduced losses and the inductance is increased. High inductance is good for achieving optimal field weakening but reduces the power factor at rated speeds. A higher PF increases the converter cost and is not an optimal solution. Using FSCW IPM has a good potential

TABLE XI: Machine variables for DL

Variable	V-IPM DL	I-IPM DL
Ψ_m [mWb]	1665	1660
L_q [mH]	0.77	0.82
L_d [mH]	0.71	0.79
FWI	1.25	1.11
PM area [m^2]	0.0157	0.0154

TABLE XII: Results from time simulation at 75 and 250 rpm double layer.

Variable	V-IPM DL	I-IPM DL
T_{avg} [kNm]	154	151
	40	54
T_{ripple} [%]	1.17	0.55
	6.21	0.32
V_{line} [V]	654	663
	534	617
THD [%]	8.79	3.63
	22.99	4.67
PF	0.81	0.79
	0.79	0.99
PM Loss [kW/m^2]	79	29
	185	176

for high field weakening applications, but comparing SPM and IPM with the same stator and split ratio is seen to be difficult.

The analyses was first based on applying SL windings, but was extended to DL windings for the IPM machines. SL windings is essential for the SPM because they provide high sub harmonic MMF, which increases the d-axis inductance and is necessary to achieve good field weakening. IPM machines do not need high sub harmonic MMF to provide high d-axis inductance. This is because the rotor outer radius can be placed closer to the stator, giving a smaller effective air gap. Applying DL winding reduce the core and PM losses significantly in both IPM designs and increases the PF due to lower machine inductance.

Both IPM machine type have the potential of performing beside and beyond the SPM machine. From the results in this paper the I-shaped IPM is showing the most promising performance concerning field weakening and losses. On the other side it must be considered that the V-shaped IPM is more complex and non-linear, making it more difficult to achieve the wanted performance. An advanced optimization algorithm is need to fully see the V-shaped IPMs potential.

The I-shaped IPM has very low PM loss. Assuming more magnet segmentation will take place in a real machine design, most of the losses will be seen on the rotor surface. Since the losses is more concentrated in the rotor core and not the PMs a new cooling technique is required. On the other hand the reduction of PM losses could increase the machine efficiency overall. Lesser loss in the PMs will reduce the temperature increase, hence keeping the remenant flux density high and less risk of demagnetization.

The IPM machines have much larger inductance then the SPM. This increases the PF as discussed. The number of turns could therefor be reduced and still have a high inductance. Reducing the number of turns will reduce copper losses. But then another optimal machine size needs to be considered. The IPM machines also have less magnet area, which will reduce the cost of the machine.

The DL winding configuration showed that there was small potential increasing the saliency of the machine. An optimal solution would be to have FSCW IPM DL winding with high saliency so the max torque angle would be in the negative d-axis. This would increase the PF at rated conditions and solve the issue high inductance brings. Several papers have studied increasing the saliency in FSCW IPMs, but with little results. However one paper [26] manipulates the saliency by changing the material at certain places in the rotor. This is an interesting concept and could be further analized.

XI. Conclusion

When designing a machine for optimal field weakening the study of d- and q-axis inductance and flux linkages is essential. FSCW SPM machines have a good ability for field weakening because of their high d-axis inductance caused by the sub harmonic MMF. However eddy current in PMs and the core reduce their ability to achieve high speeds.

Both SL and DL winding configurations are good choices for FSCW IPM machines when it comes to field weakening. In this paper some issues accrued with the V-shaped IPM having high torque ripple or high PM loss. It seems to be a trade off between them depending on the magnet height. The I-shaped IPM shows the best results between all the IPM designs. Reducing losses in the PMs significantly and as well having low ripple and THD. The only drawback is the low PF, which can be fixed with DL winding in this case.

Achieving optimal field weakening has its downside on the converter. High inductance leads to low PF and increases the cost. But this can maybe be used to its advantage by changing for instance the size or number of turns in the machine. This has not been studied further in this paper, but could be interesting to investigate further.

References

[1] A. M. El-Refaie and T. M. Jahns, "Optimal flux weakening in surface pm machines using concentrated windings," in *Industry Applications Conference, 2004. 39th IAS Annual Meeting. Conference Record of the 2004 IEEE*, vol. 2. IEEE, 2004, pp. 1038–1047.

[2] A. M. El-Refaie, T. M. Jahns, and D. W. Novotny, "Analysis of surface permanent magnet machines with fractional-slot concentrated windings," *IEEE Transactions on Energy conversion*, vol. 21, no. 1, pp. 34–43, 2006.

[3] A. M. El-Refaie, T. M. Jahns, P. J. McCleer, and J. W. McKeever, "Experimental verification of optimal flux weakening in surface pm machines using concentrated windings," *IEEE Transactions on Industry Applications*, vol. 42, no. 2, pp. 443–453, 2006.

[4] W. L. Soong and T. Miller, "Field-weakening performance of brushless synchronous ac motor drives," *IEE Proceedings-Electric Power Applications*, vol. 141, no. 6, pp. 331–340, 1994.

[5] Y. Honda, T. Nakamura, T. Higaki, and Y. Takeda, "Motor design considerations and test results of an interior permanent magnet synchronous motor for electric vehicles," in *Industry Applications Conference, 1997. Thirty-Second IAS Annual Meeting, IAS'97., Conference Record of the 1997 IEEE*, vol. 1. IEEE, 1997, pp. 75–82.

[6] J. K. Tangudu and T. M. Jahns, "Comparison of interior pm machines with concentrated and distributed stator windings for traction applications," in *2011 IEEE Vehicle Power and Propulsion Conference*. IEEE, 2011, pp. 1–8.

[7] D. C. Hanselman, *Brushless permanent magnet motor design*. The Writers' Collective, 2003.

[8] S. Skaar, O. Krovel, and R. Nilssen, "Distribution, coil-span and winding factors for pm machines with concentrated windings," *ICEM 2006*, pp. 2–5, 2006.

[9] D. Nguyen, R. Dutta, J. Fletcher, F. Rahman, and H. Lovatt, "Performance analysis of a new concentrated winding interior permanent magnet synchronous machine under field oriented control," in *2014 International Power Electronics Conference (IPEC-Hiroshima 2014-ECCE ASIA)*. IEEE, 2014, pp. 2679–2685.

[10] N. Bianchi and M. Dai Prè, "Use of the star of slots in designing fractional-slot single-layer synchronous motors," *IEE Proceedings-Electric Power Applications*, vol. 153, no. 3, pp. 459–466, 2006.

[11] D. Žarko, D. Ban, and R. Klarić, "Finite element approach to calculation of parameters of an interior permanent magnet motor," *AUTOMATIKA: časopis za automatiku, mjerenje, elektroniku, računarstvo i komunikacije*, vol. 46, no. 3-4, pp. 113–122, 2006.

[12] D. M. Ionel, M. Popescu, S. J. Dellinger, T. Miller, R. J. Heideman, and M. I. McGilp, "On the variation with flux and frequency of the core loss coefficients in electrical machines," *IEEE Transactions on Industry Applications*, vol. 42, no. 3, pp. 658–667, 2006.

[13] T. Reichert, T. Nussbaumer, and J. W. Kolar, "Split ratio optimization for high-torque pm motors considering global and local thermal limitations," *IEEE Transactions on Energy Conversion*, vol. 28, no. 3, pp. 493–501, 2013.

[14] B. Hu Li, T. Xiao, L. Zhang, A. M. EL-Refaie, Z. Zhu, T. M. Jahns, and D. Howe, "Winding inductances of fractional slot surface-mounted permanent magnet brushless machines," *COMPEL-The international journal for computation and mathematics in electrical and electronic engineering*, vol. 28, no. 6, pp. 1590–1606, 2009.

[15] L. Dupré, P. Dr Guillaume Crevecoeur, J. Seok Choi, T. Yamada, K. Izui, S. Nishiwaki, H. Lim, and J. Yoo, "Optimal shape design of flux barriers in ipm synchronous motors using the phase field method," *COMPEL: The International Journal for Computation and Mathematics in Electrical and Electronic Engineering*, vol. 33, no. 3, pp. 998–1016, 2014.

[16] R. Dutta and M. Rahman, "Design and analysis of an interior permanent magnet (ipm) machine with very wide constant power operation range," *IEEE Transactions on Energy Conversion*, vol. 23, no. 1, pp. 25–33, 2008.

[17] S. Chaithongsuk, N. Takorabet, and S. Kreuawan, "Reduction of eddy-current losses in fractional-slot concentrated-winding synchronous pm motors," *IEEE Transactions on Magnetics*, vol. 51, no. 3, pp. 1–4, 2015.

[18] Y.-Y. Choe, S.-Y. Oh, S.-H. Ham, I.-S. Jang, S.-Y. Cho, J. Lee, and K.-C. Ko, "Comparison of concentrated and distributed winding in an ipmsm for vehicle traction," *Energy Procedia*, vol. 14, pp. 1368–1373, 2012.

[19] A. Masmoudi, A. M. EL-Refaie, and T. M. Jahns, "Comparison of synchronous pm machine types for wide constant-power speed range operation," *COMPEL-The international journal for computation and mathematics in electrical and electronic engineering*, vol. 27, no. 5, pp. 967–984, 2008.

[20] Y. Lu, J. Li, R. Qu, and A. Sun, "Design and analysis of a hybrid permanent magnet variable-flux flux-intensifying machine," in *Electrical Machines and Systems (ICEMS), 2016 19th International Conference on*. IEEE, 2016, pp. 1–6.

[21] H. Haugdal, "Developing an application for simulating a parametrized pm machine by fem," 2016.

[22] A. Lagerström, "Design of large pm-generators for wind power applications," Master's thesis, NTNU, 2011.

[23] J. Lavers, P. Biringer, and H. Hollitscher, "A simple method of estimating the minor loop hysteresis loss in thin laminations," *IEEE Transactions on magnetics*, vol. 14, no. 5, pp. 386–388, 1978.

[24] A. Brockmeyer, "Experimental evaluation of the influence of dc-premagnetization on the properties of power electronic ferrites," in *Applied Power Electronics Conference and Exposition, 1996. APEC'96. Conference Proceedings 1996., Eleventh Annual*, vol. 1. IEEE, 1996, pp. 454–460.

[25] "Steel lamination data: M400 50a," http:https://www.emetor.com/edit/materials/sura-no20/, accessed: 2017-05-27.

[26] L. Yue, P. Yulong, Y. Yanjun, S. Yanwen, and C. Feng, "Increasing the saliency ratio of fractional slot concentrated winding interior permanent magnet synchronous motors," *IET Electric Power Applications*, vol. 9, no. 7, pp. 439–448, 2015.

APPENDIX A
MATLAB CODE: MAIN LOSS SCRIPT

```
clc;
clear;
close all;


% Simulations Without PM loss included

FileLocation{1}='C:\Users\PALASSE\Google Drive\
    MasterOppgave\Comsol\RefereranseMotor\SPM_75Free
    ';

% % Simulations With PM loss included
FileLocationPM{1}='C:\Users\PALASSE\Google Drive\
    MasterOppgave\Comsol\RefereranseMotor\SPM_75';

% %File name
name{1}='SPM 75 rpm';


%%
% Fetch curve fitted steel lamination data
[ Ke,Ka,Kh,Blim,fVals,rho] = M400_50A();
% Initiat waitbar
global h;
h=waitbar(0,'Begining Calculations...');

%%
N=length(FileLocation);

for i=1:1:N

mphopen(FileLocation{i});

% Get general variables and results
[symmetry,length]=mphglobal(model,{'symComp','L'},'t
    ',0,'dataset','dset31');
[V{i},Torque{i},phi{i}]=mphglobal(model,{'Va','-rmm.
    Tz_Frot*symComp*L/1[m]','phi'},'dataset','dset31
    ');

%Compute Stator Loss (Hysteresis, eddy current and
    excess loss)
waitbar(i/N,h,'Stator Loss');

[Pe,Ph] = calculateLoss(model,'uni25',40,Ke,Ka,Kh,
    Blim,fVals,rho );
CoreLossStator(i)=(sum(Pe)+Ph)*(symmetry*length);

%Compute Rotor Loss (eddy current and excess loss)
waitbar(i/N,h,'Rotor Loss');

[Pe,Ph] = calculateLoss( model,'uni24',40,Ke,Ka,Kh,
    Blim,fVals,rho );
CoreLossRotor(i)=(sum(Pe)+Ph)*(symmetry*length);
%
%Get PM loss from model
 mphopen(FileLocationPM{i});
 waitbar(i/N,h,'PM Loss');

 PMLoss=mpheval(model,'rmm.Qrh*symComp*L','selection
     ','uni5','pattern','gauss','dataonly','on','
     dataset','dset31');
 area = mpheval(model,'dvol/2','selection','uni5','
     pattern','gauss','dataonly','on','dataset','
     dset31');
```

```
 PMLoss=PMLoss.*area;
 PMLoss=sum(PMLoss,2);
 PMarea=sum(area,2);
 PMvol=length*symmetry*PMarea(1);

 %Total loss
 PMEddyLoss(i)=mean(PMLoss(2:end));
 %Spesefic loss
 PMSpesLoss(i)=PMEddyLoss(i)/PMvol;

end

delete(h);
```

MATLAB CODE: LOSS FUNCTION

```
function [ Z,X ] = calculateLoss( model,domain,Nh,Ke,Ka,Kh,Blim,fVals,rho )
%
% Pattern= gauss to avoid getting several points in one meshelement
% dvol = meshelement volume factor
% since alle meshelements have 3 point (triangles)
% finding the area of one meshelement is easy
% area=dvol*1/2
% uni25 : Stator Core
% uni24 : Rotor Core
global h;
% uni5 : PM all


data= mpheval(model,{'dvol/2','rmm.Bx','rmm.By','t','w'},'selection',domain,'pattern','gauss','dataonly','on','dataset','dset31');
area=data.d1;
Bx=data.d2;
By=data.d3;
t=data.d4;
w=data.d5;
f_fund=w(20,1)/(2*pi);

Ts=t(20,1)-t(19,1);
Fs=1/Ts;
L=length(area(:,1));
%rho = 7600; %kg/m^3


% Finding Flux density direction for each point
[Nt,Nn]=size(t);

%Nh=20; %number of harmonics to include in analyse

P=zeros(Nn,Nh);
Ph=zeros(Nn,1);
for i=1:1:Nn
waitbar(i/Nn,h);

absB(:,i)=sqrt(Bx(:,i).^2+By(:,i).^2);

% find max absolutt value of B
max=0;
maxIndex=1;
for j=1:1:Nt
    if absB(j,i)>max
    maxIndex=j;
    max=absB(j,i);
    end
end

%change from xy-plane to the found reference angle
BmaxIndex(i)= maxIndex;

if By(BmaxIndex(i),i) < 0 && Bx(BmaxIndex(i),i)< 0
theta(i)=atan(By(BmaxIndex(i),i)/Bx(BmaxIndex(i),i))+pi;
elseif By(BmaxIndex(i),i) > 0 && Bx(BmaxIndex(i),i)< 0
theta(i)=atan(By(BmaxIndex(i),i)/Bx(BmaxIndex(i),i))+pi;
else
theta(i)=atan(By(BmaxIndex(i),i)/Bx(BmaxIndex(i),i));
end

Bdata(:,i)= Bx(:,i).*cos(theta(i))+By(:,i).*sin(theta(i));

df=Fs/Nt;
Y(:,i) = fft(Bdata(:,i))/L;
f(:,i) = (0:df:Fs/2);
if size(f,1)<Nh
    Nh=size(f,1);
end

%get element total loss based on harmonics for hysteresis and excess loss!
for j=1:1:Nh
 P(i,j)=P(i,j)+getLoss(f(j,i),2*abs(Y(j,i)),Ke,Ka);
end

%Hysteresis loss without minor loops!

Ph(i)=Ph(i)+getHystLoss(f_fund,Bdata(maxIndex,i),Kh,Blim,fVals);
Ph(i)=Ph(i)*(rho*area(1,i));
P(i,:) = P(i,:).*(rho*area(1,i));

end

Z=sum(P);
X=sum(Ph);

end
```

MATLAB CODE:CURVE FIT TO LOSS DATA

```
function [ Ke,Ka,Kh,Blim,fVals,rho ] = M400_50A()

% Manufacturer data to fit
f=[50 100 200 400 1000];
B=0.1:0.1:1.8;
loss(1,:)=[0.02 0.09 0.19 0.31 0.46 0.62 0.81 1.01 1.24 1.49 1.76 2.09 2.46 2.96 3.57 4.38 5.02 5.47];
loss(2,:)= [0.07 0.26 0.54 0.88 1.27 1.73 2.24 2.8 3.44 4.15 4.95 5.85 6.88 8.18 9.82 -1 -1 -1];
loss(3,:)= [0.16 0.64 1.35 2.25 3.33 4.58 6.03 7.68 9.58 11.7 14.2 17 20.2 23.8 28.3 -1 -1 -1];
loss(4,:)= [0.48 1.8 3.77 6.29 9.37 13.1 17.5 22.7 28.8 35.9 44.2 53.8 64.9 77.4 91.7 -1 -1 -1];
loss(5,:)= [2.12 7.49 15.3 25.7 39 56.1 77.1 103.1 135 173.3 218.8 272.4 334.6 405.6 488.4 -1 -1 -1];
loss(6,:)=[8.64 30.1 62.7 109 172 256 367 509 685 899 1145 1453 1793 2130 -1 -1 -1 -1];
rho=7600; %mass density of the steel

N_freq=length(f);
N_B=15;

%% STEP 1
%Perform quadratic curve fitt and get a,b,c
for i=1:1:N_B

%Fetch current data
P=loss(1:N_freq,i);

% count data
N_data=N_freq;
```

```
for j=1:1:N_freq
    if P(j)==-1
    N_data=N_data-1;
    end
end

% Must have at least five datapoints to get good
    estimations
if N_data>=5
    P=P(1:N_data);
    %Scale
    y=P./f(1:N_data)';

    x=sqrt(f(1:N_data))';
    fitt = fit(x,y,'poly2');

    a(i)=fitt.p3;
    b(i)=fitt.p2;
    c(i)=fitt.p1;

end

end

%c = Ke*B^2
%b = Ka*B^1.5
%a = Kh*B^alpha



%% STEP 2

% Find Ke and Ka with curve fit
Ke = fit(B(1:length(c))',(c./(B(1:length(c))).^2))','
    poly3');
Ka = fit(B(1:length(b))',(b./(B(1:length(b))).^1.5))
    ','poly3');


%% STEP 3


 %Fetch current data

for j=1:1:N_freq

  for i=1:1:N_B
      Pe=Ke(B(i))*B(i)^2*f(j)^2;
      Pa=Ka(B(i))*B(i)^1.5*f(j)^1.5;

     a_new(j,i)=(loss(j,i)-Pe-Pa)/f(j);

%      if a_new(j,i)<0
%          a_new(j,i)=1e-4;
%      end
  end

end


%% STEP 4

% define range based on recent plot
B1=0.4;
B11=0.4;
B2=0.8;
B3=0.8;
n1=0;
n2=0;
n3=0;
for j=1:1:N_freq
for i=1:1:N_B
    K=log(B(i));

    if B(i)<B1
        n1=1+n1;
        Bmatrix1(n1,:)=[1 K];
        A1(n1)=log(a_new(j,i));
    end

    if B(i)>=B11 && B(i)<=B2
        n2=1+n2;
        Bmatrix2(n2,:)=[1 K];
        A2(n2)=log(a_new(j,i));
     end

    if B(i)>=B3
        n3=1+n3;
        Bmatrix3(n3,:)=[1 K];
        A3(n3)=log(a_new(j,i));
    end

end

Y1=Bmatrix1\A1';
Y2=Bmatrix2\A2';
Y3=Bmatrix3\A3';

Kh1(j,1)=exp(Y1(1));
Kh2(j,1)=exp(Y2(1));
Kh3(j,1)=exp(Y3(1));
Kh1(j,2)=Y3(2);
Kh2(j,2)=Y2(2);
Kh3(j,2)=Y3(2);

end

Kh={Kh1 Kh2 Kh3};
Blim=[B1 B11 B2 B3];
fVals=f;

end
```